



## CHAPTER IV

### RESULTS AND DISCUSSION

Discussion of the results obtained from this work is divided into two main parts. The first section deals mainly on the raw material preparation and characterization while the later section focuses on the thermal degradation of prepared samples at various conditions. The utilization of findings from this work is also included afterward in the chapter.

#### 4.1 Biodegradable additive determinations

##### 4.1.1 Yield of microcrystalline cellulose

Bleached cotton fabric was subjected to acid hydrolysis reaction in order to produce microcrystalline cellulose. Table 4.1 presents weight of bleached cotton fabric before and after hydrolysis. In this experiment, 5 replicated runs of acid hydrolysis were performed and the average dry weight of microcrystalline cellulose was measured. The average yield of microcrystalline cellulose among these experiments was 61.07%.

Table 4.1 Weight of bleached cotton fabric before and after hydrolysis

Weight before hydrolysis (g)	Weight after hydrolysis (g)	% Yield
25.04	15.52	61.98
25.10	15.47	61.63
25.07	15.40	61.43
25.09	15.12	60.26
25.11	15.08	60.06
		Average 61.07%

#### 4.1.2 Morphology of biodegradable additives

Scanning electron microscope (SEM) of cassava starch and microcrystalline cellulose was carried out to investigate the morphology of raw materials. Figure 4.1 shows a scanning electron micrograph of these two materials. From naked eyes, both of them seem to be in powdery form but from SEM analysis, microcrystalline cellulose exhibited a microfibril structure with an average diameter and length of 10  $\mu\text{m}$  and 70  $\mu\text{m}$ , respectively (Figure 4.1b and 4.1d). However, under SEM microscope, the starch granule shows round, spherical shape with corresponding diameter of approximately 15  $\mu\text{m}$  (Figure 4.1a and 4.1c).

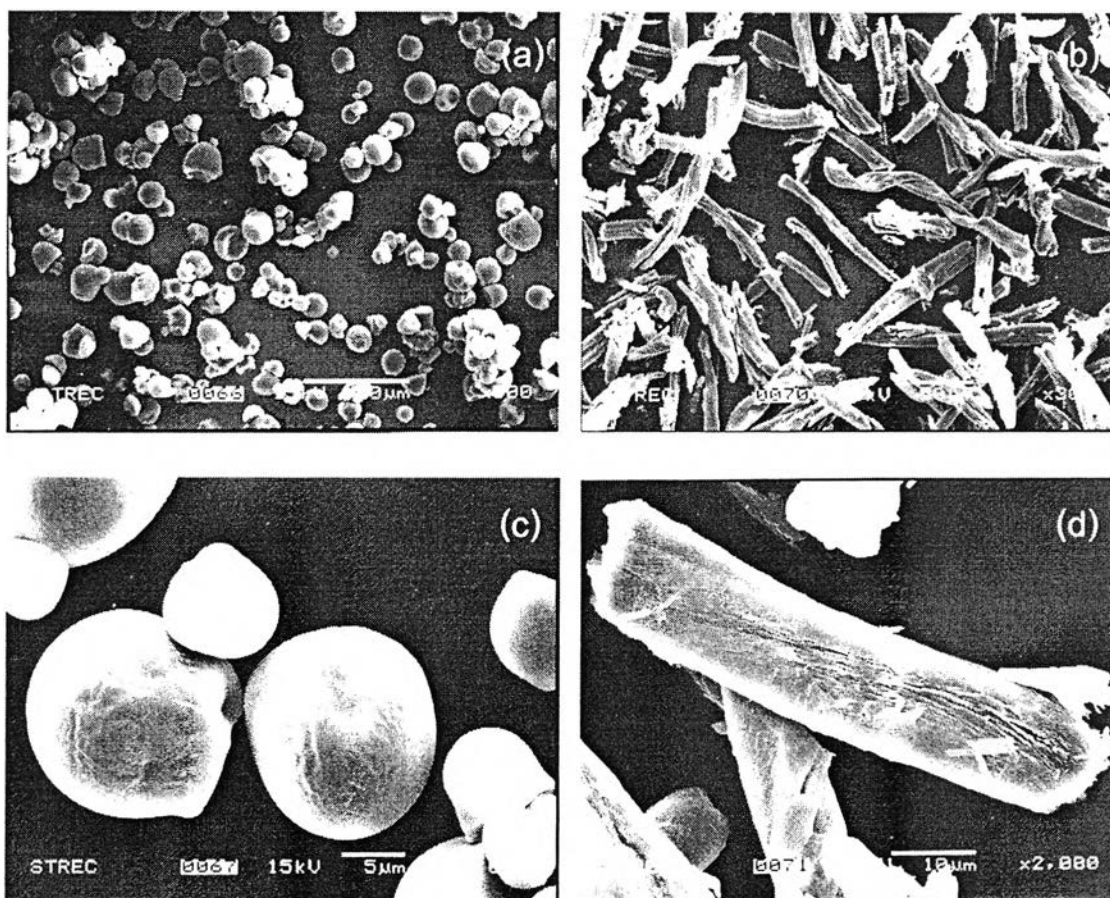


Figure 4.1 Scanning electron micrograph of cassava starch (a) and microcrystalline cellulose (b) with the detailed morphology in (c) and (d), respectively.

#### 4.1.3 Elemental composition of biodegradable additives

The elemental composition of additives was performed using elemental analyzer. Table 4.2 shows the elemental compositions of these biodegradable additives. From this table, it can be seen that the composition of C, H, N, O in both additives are quite similar. It is due to the fact that repeating unit of both starch and cellulose is glucose. The difference between starch and cellulose is only the bond linkage between each glucose unit. For the case of starch, linkage is  $\alpha$ -(1,4) and  $\alpha$ -(1,6) linked. But the linkage in cellulose is instead the  $\beta$ -(1,4)-linked (Shlieout *et al.*, 2002).

The ratio of elemental compositions of starch and cellulose obtained by elemental analysis technique in C : H : N : O are 28.05 : 51.42 : 0.14 : 20.25 and 29.01 : 49.92 : 0.27 : 20.35 respectively. The number is acceptable when compared with the ratio from empirical molecular formula of starch and cellulose which are  $(C_6H_{10}O_5)_x$ .

This information in elemental compositions of each biodegradable additive will be used to compare with the elemental analysis data of char residue after pyrolysis process occurred and also for calculation of the degree of conversion from this thermal degradation which will be discussed further in section 4.2.2.

Table 4.2 Elemental compositions of cassava starch and microcrystalline cellulose

Elemental composition	C	H	N	O
Starch	28.05	51.42	0.14	20.08
Cellulose	29.01	49.92	0.27	20.35

#### 4.1.4 Physical appearance of biodegradable composites

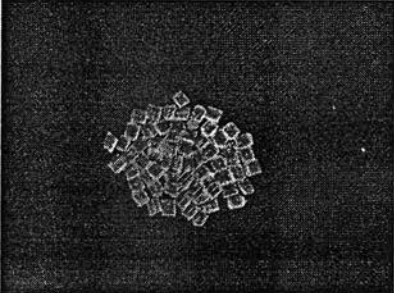
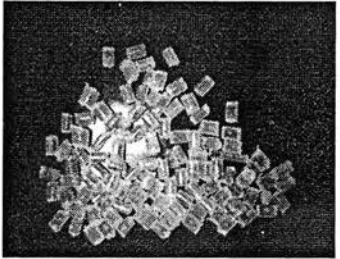
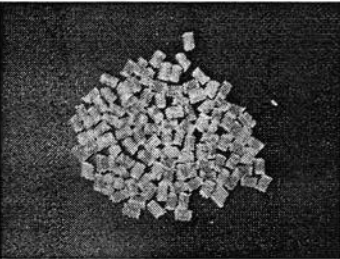
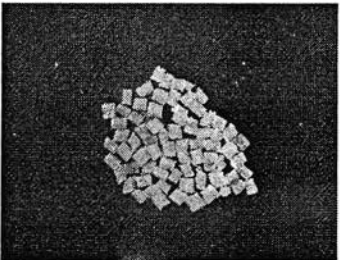
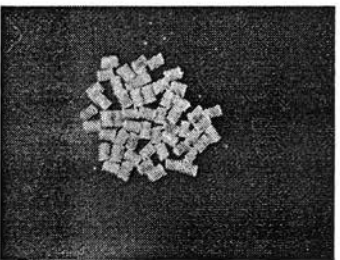
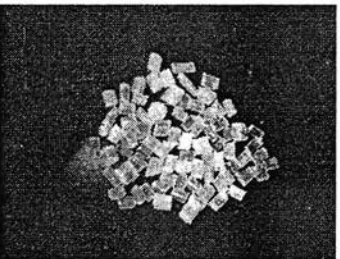
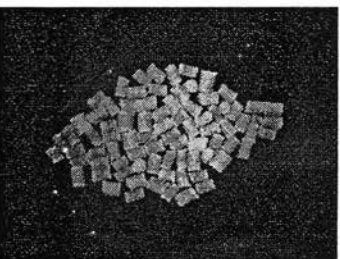

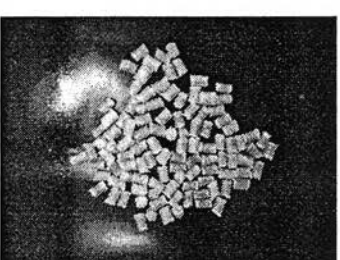
Table 4.3 shows the physical appearance of biodegradable composites of polypropylene (PP) with cassava starch (STR) or microcrystalline cellulose (MCC). Closer look of these pictures revealed the roughness surface of composites in higher additive compositions (15 and 20%). It might be due to the non-polar property of PP polymer and

the polar STR and MCC counterparts which makes these substances incompatible to some extent.

The PP/STR composites show white color in all starch compositions. But in PP/MCC composites, it exhibits yellowish color in the 15 and 20% MCC compositions. While consider the decomposition profile of starch and cellulose applied by TGA from Figure 4.3 in section 4.2.1, it can be shown from DTG curves that the maximum rate of decomposition of starch and cellulose occurred at 330 and 372°C, respectively. From this data, the processing temperature of PP/biodegradable additives read out by twin screw extruder is around 160–170°C which is not likely to be the reason of yellowish color in PP/MCC composites. However, the TGA data yields only the change in mass of a decomposed sample but the change in chemical structure and physical appearance are not considered. So the TGA data couldn't be conferred as the reason for MCC decomposition during composites process.

When consider the activation energy of starch and cellulose applied further in section 4.2.3, it can be shown that  $E_a$  of starch and cellulose is 370.02 and 233.4 kJ/mol, respectively. It can be inferred from these values presented from the Table 4.12 that cellulose exhibits lower activation energy which indicates lesser thermal stability compared to starch. It might be due to microcrystalline cellulose is cellulose with isolated crystal region. This rigid framework might be broken down easily than the more flexible structure of starch. This might result in the bond breaking in cellulose that leads to the yellowish color appear in PP/MCC composites.

Table 4.3 Physical appearance of biodegradable composites

% of biodegradable additives	Starch	Cellulose
0		
5		
10		
15		
20		

## 4.2 Thermal degradation studies by pyrolysis process

### 4.2.1 Decomposition profiles of PP and its composites

A preliminary analysis of the thermal behavior of pure PP was carried out using three different sample sizes (10, 20 and 30 mg) at a heating rate of 20°C/min in order to determine the reproducibility of the experiment and sensitivity of the results with regards to sample size and heat transfer limitation, if any. The resulting TGA thermograms of PP displayed in Figure 4.2 (a) compared the decomposition profiles of PP at different sample sizes along with their respective DTG thermograms (b) which may be used to determine the decomposition rate of PP at any instance.

The TGA curves of PP exhibited one main distinct weight loss step, which showed that PP has a constant degradation behavior at the interested temperature range and sample sizes. From the DTG curves, it can be seen that the onset of the decomposition temperature of PP at three different sample sizes was approximately 400°C. In addition, upon increasing the temperature, weight loss of all sample sizes continually increased up to about 500°C where all the TGA thermograms showed complete weight loss of samples. In other words, no char residue can be observed in thermal decomposition of PP even without addition of oxidizing agent.

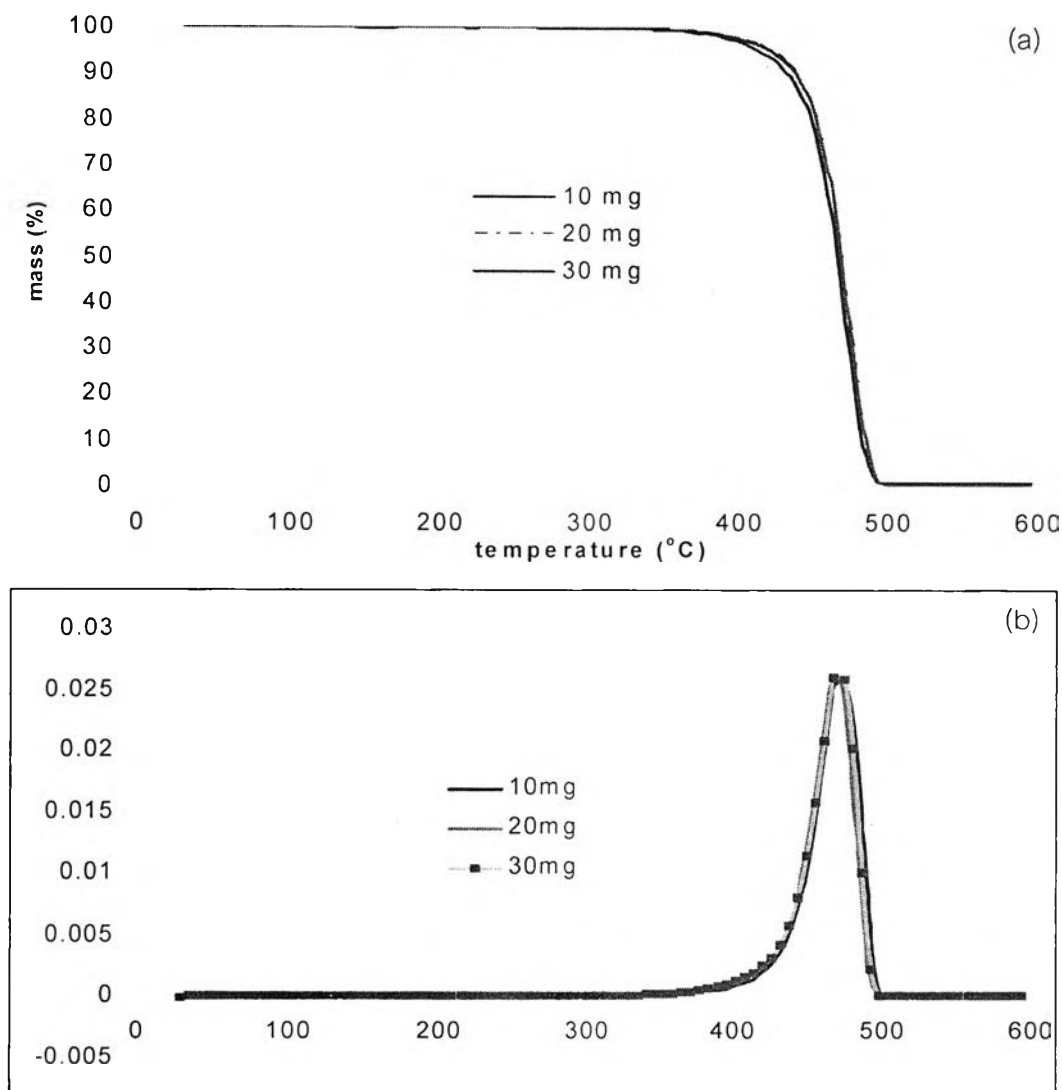


Figure 4.2. Reproducibility of the TGA (a) and DTG (b) curves of PP decomposition.

Figure 4.3 is a comparison of the decomposition profiles of PP and biodegradable additives (STR and MCC) at a heating rate of 20°C/min. It can be seen that both starch and cellulose exhibited an initial weight loss of 12 and 5%, respectively, at around 100°C. This appeared to be due to the moisture released from microcrystalline cellulose which has more rigid framework that can absorb less bound water when compared with starch. Negligible weight loss of PP at 100°C may be due to its non-polar behavior which does not support adsorption of moisture to its structure. This figure also shows that STR and MCC decomposed at a lower temperature than PP with the onset value of decomposition temperature of 290, 300, and 400°C on STR, MCC, and PP,

respectively. The greater decomposition temperature of MCC than that of STR might be due to the more rigid crystal structure of MCC. When compare with PP, the obstructively long chain polymeric structure should be decomposed to volatile products at higher temperature compare with biodegradable additives. Unlike PP, both STR and MCC thermograms showed slow charring reaction of biodegradable additives continuing in the temperature range of polymer decomposition until the end of the experiment leaving remained char residue. These char formation might influence the decomposition behavior of PP which will be discussed further in section 4.2.

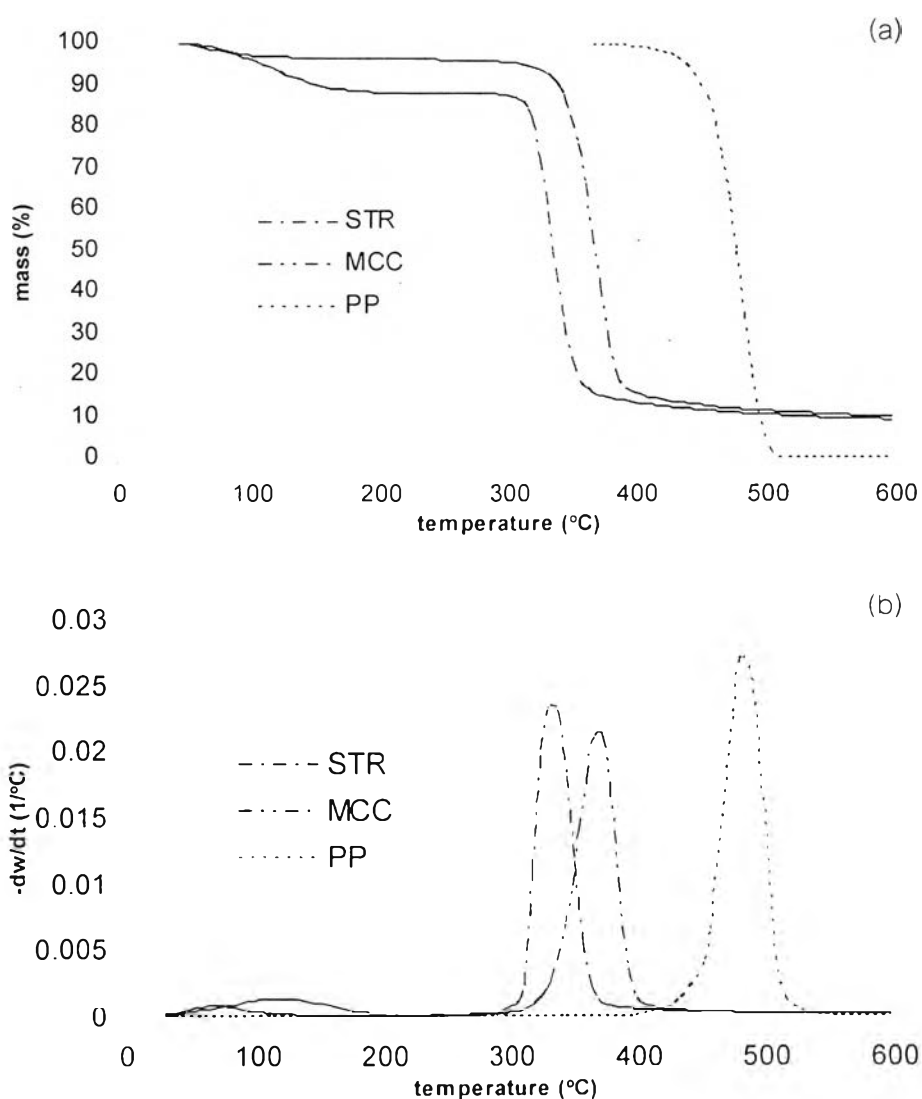


Figure 4.3. TGA (a) and DTG (b) curves of PP, STR and MCC.



In order to determine the effect of biodegradable additives on thermal behavior of PP, PP/STR and PP/MCC composites, the thermal decomposition profile of PP and its composites at various compositions were studied. The decomposition profile of PP/STR and PP/MCC composites at different compositions are given in Figure 4.4 and 4.5, respectively. Figure 4.4 shows that upon increasing starch content from 5 to 20% weight loss due to moisture at approximately 100°C were slightly increased. When compared with TGA curves of pure starch in Figure 4.3, this initial weight loss was less pronounced due to the PP matrix that prevented the moisture release. Similarly, the char residue was also increased when the amount of starch in the PP composites increased. However, the starch content had no effect on the onset of decomposition temperature ( $T_d$ ). The  $T_d$  onset of PP in the presence of various amount of starch remained constant at approximately 400°C compare to pure PP in Figure 4.2. The similar trends of initial weight loss of MCC at 100°C and  $T_d$  onset of PP in the presence of cellulose were observed as shown in Figure 4.5.

As mentioned earlier, the decomposition of biodegradable additives precedes that of PP. It can be seen that two steps of decomposition occurred in TGA curves of PP composites. As the additives level increase, the weight loss corresponding to the decomposition of additives increase. This behavior suggests that the presence of char residue might have some influence on the polymer decomposition. As seen in Fig. 4.4 and 4.5, char residue from starch and cellulose can accelerate the thermal decomposition of PP by shifting the maximum rate of decomposition to lower temperature by 12 and 10°C, respectively. The effect of char residue on the pyrolysis products was determined in next section.

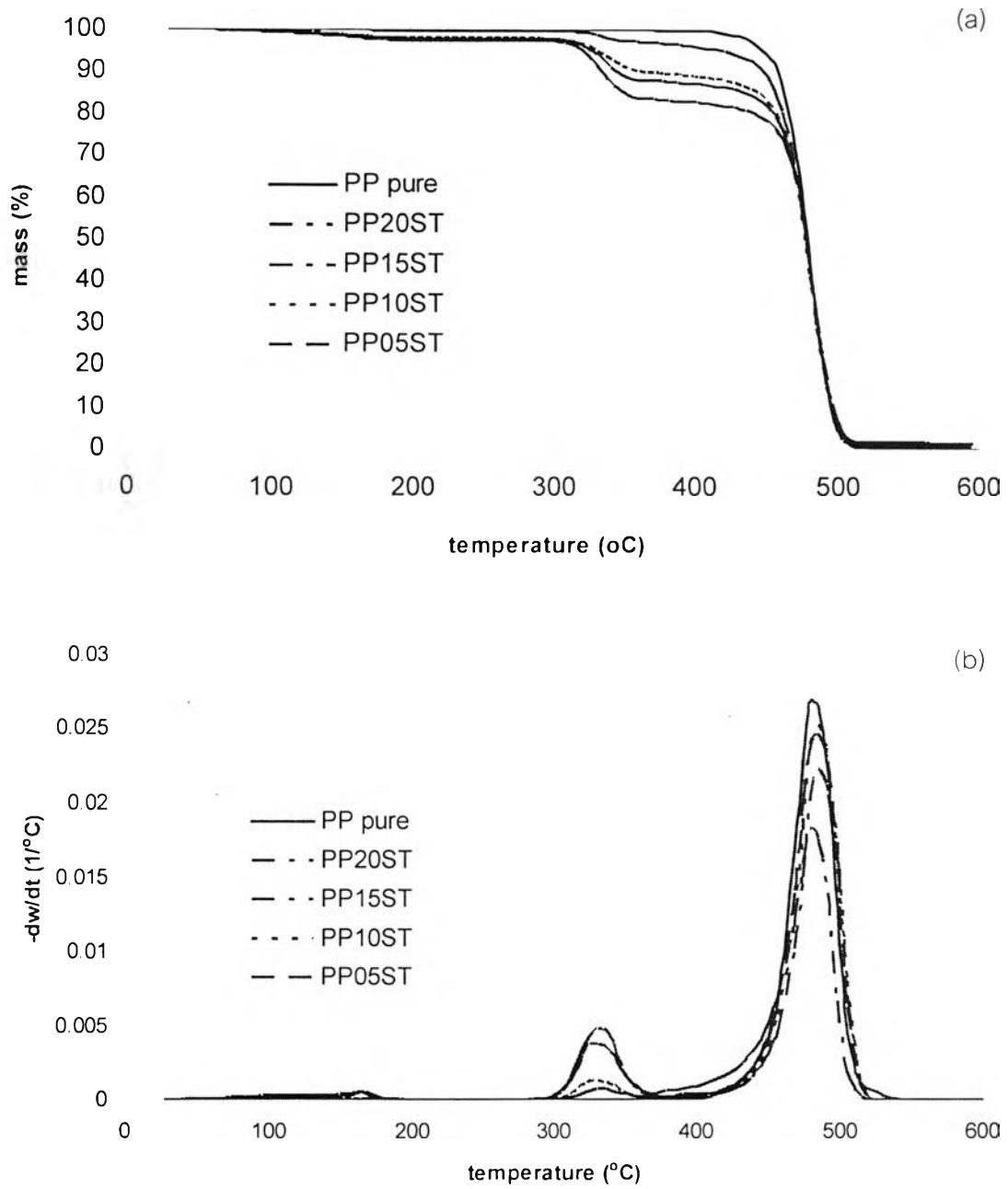


Figure 4.4. Comparison of TGA (a) and DTG (b) curves of PP and PP/STR.

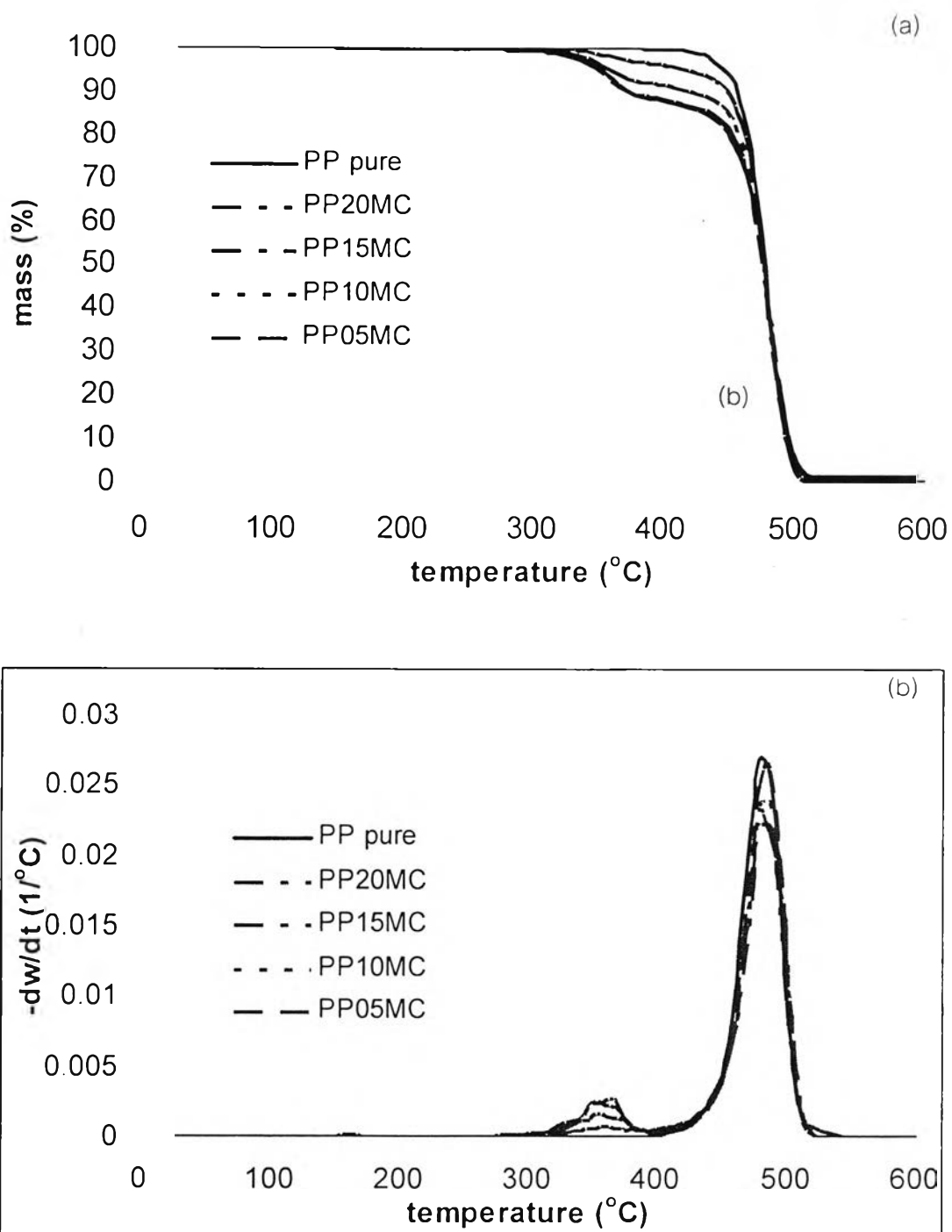


Figure 4.5. Comparison of TGA (a) and DTG (b) curves of PP and PP/MCC.

#### 4.2.2 Pyrolysis products determination

Pyrolysis of PP and its corresponding biodegradable composites was performed in order to investigate the influence of biodegradable additives on pyrolysis products compared to pure PP. The initial weight of each sample was about 30 mg. The amount of cellulose and starch in the composites were varied from 5 to 20%. The temperature program on the TGA was initially from 30°C and gradually heated with a fixed heating rate varied from 10, 20, or 30°C/min. The ceiling temperature was maintained at 600°C and applied in all experiment. During each run, 50 ml/min of high purity nitrogen was used as carrier gas to maintain pyrolysis condition within the reaction chamber and also to flush products out of the furnace for further analysis. Gas products were collected in several Tedlar<sup>®</sup> gas sampling bags. The identification of gas products obtained was performed immediately by injecting sample into gas chromatography-mass spectrometry (GC-MS) using the condition described in previous chapter. It was found that most of the liquid products condensed in the gas transfer line so dichloromethane was used to dissolve all of the condensed products prior to GC-MS analysis.

Figure 4.6 shows product yield of PP composites compared to that of PP. Char residue remained in sample holder and liquid product condensed from the transfer line of TGA were weighted. The amount of gaseous products was calculated by subtracting the weight of liquid products and char residue from the total weight of sample initially loaded to the TGA. It can be seen that liquid yield was a major fraction when compared to gas and char residue in all sample ranging more than 60% of total mass in most cases. Total gas product obtained was around 33-38% while only few weight percents recovered as char residue.

Pure PP produced only gas and liquid fraction without any residue. The gas and liquid yield was 34 and 66%, respectively. After application of biodegradable additives into PP, some char residues were remained presumably from those additions. Also gas yield from PP composites was increased with the consequent decrease in liquid yield. This change might be the result of the char residue from biodegradable additives affected the decomposition mechanism of PP. When compare the effect of starch with cellulose on product yield, starch has more pronounced effect on the PP decomposition

than cellulose, but similar tendencies can be observed. It might be due to the amount of char remaining from starch is greater than cellulose, for example in 20% additives, starch produces 2.7% char compared with the 2.3% char from cellulose.

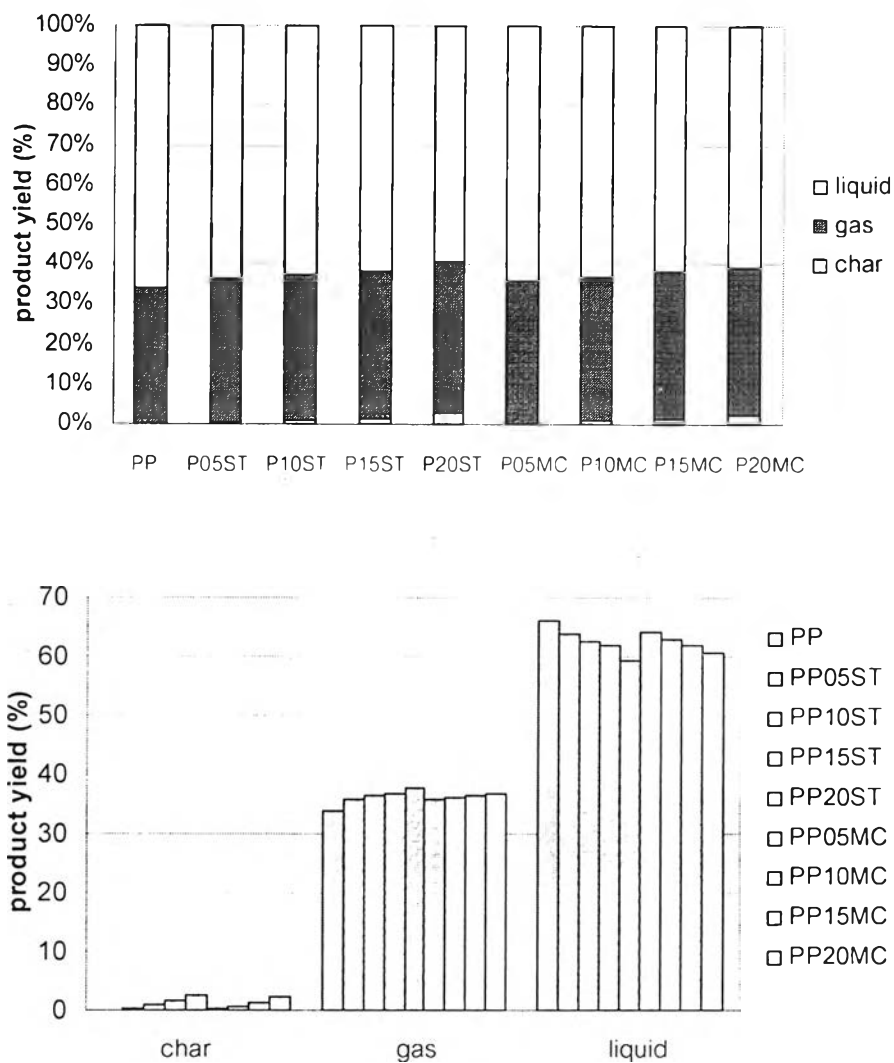


Figure 4.6 Product yields of PP composites in various compositions.

Next, each type of product was analyzed in detailed in order to identify the pyrolysis products. Char residue remained in sample holder were further characterized to compare with virgin biodegradable additives previously analyzed in section 4.1 using scanning electron microscopy and elemental analysis to determine morphology and elemental composition, respectively.

Gas product was collected in gas sampling bag but liquid product trapped on the output of TGA was eluted by dichloromethane which used as solvent. Both gas and liquid products were analyzed by GC-MS to perform a qualitative study to identify each separated component by match the MS-spectrum from experiment with the available MS-spectrum library. A quantitative study was also performed using gas chromatography (GC) by calculate an area percent of each separated component as presented in Equation 4.1.

$$\text{Area percent of component X} = \frac{\text{Area of component X}}{\text{Total area of all components}} \times 100 \quad (4.1)$$

Figure 4.7 shows the example of gas chromatograms of pyrolysis products of PP liquid yield compared with gas yield. Additionally, Figure 4.8 and Figure 4.9 show comparison of gas yield from PP composites at 5 and 20% additive contents of starch and cellulose, respectively. Each separated peak was identified by GC-MS and area% of each peak was analyzed by GC. The example of products identification by matched the mass spectrum from the separated peak with mass spectrum from library is shown in Figure 4.10. From these chromatograms, pyrolysis products of PP and PP composites in various amounts of biodegradable additives were identified and summarized in Table 4.4–4.7. In this classification, low-molecular weight hydrocarbons (from C<sub>3</sub>–C<sub>6</sub> such as propane, propene, butane, and isobutane) were combined into one group, as gaseous products. The higher-molecular weight hydrocarbons (more than C<sub>7</sub> such as heptane, octane, and 2,6-dimethyl-nonane) were also combined into another group, as liquid products.

As reviewed earlier, a thermal degradation mechanism of PP is considered as radical processes. After the bond scission occurred, subsequent beta-scission leads to an alkene and additional radical species. These radical are saturated via hydrogen transfer resulting in alkanes. Though low alkane concentration in pyrolysis products of PP indicating that hydrogen transfer reactions might be absence (Ballice and Reimert, 2002).

It can be observed from Table 4.4–4.7 that the pyrolysis product distribution changes significantly in the presence of 5 to 20% biodegradable additives. The total yield of higher molecular weight products from PP compared with PP composites at 20% starch decreased 6.6% from 66.1 to 59.5%. When compare with PP/MCC at 20% cellulose, the presence of cellulose had decreasing influence on the liquid fraction from 66.1% in pure PP to 60.8% in PP/MCC composites with 5.3% reduction. This effect might be proportional to less char yields from cellulose compare with starch in the value of 2.3 and 2.7%, respectively.

In contrast, char residue from biodegradable additives promoted the formation of lower molecular weight products from 33.9 to 37.8% in the presence of 20% starch. The similar trends may be noticed in the presence of cellulose. In this case, gas fraction from pyrolysis of PP/MCC at 20% additives increased 3% from 33.9 to 36.9%. It means that more radical decomposition occurred resulting in the further breakdown of PP polymer into lower molecular weight products in the presence of char residues (Jakab *et al.*, 2000).

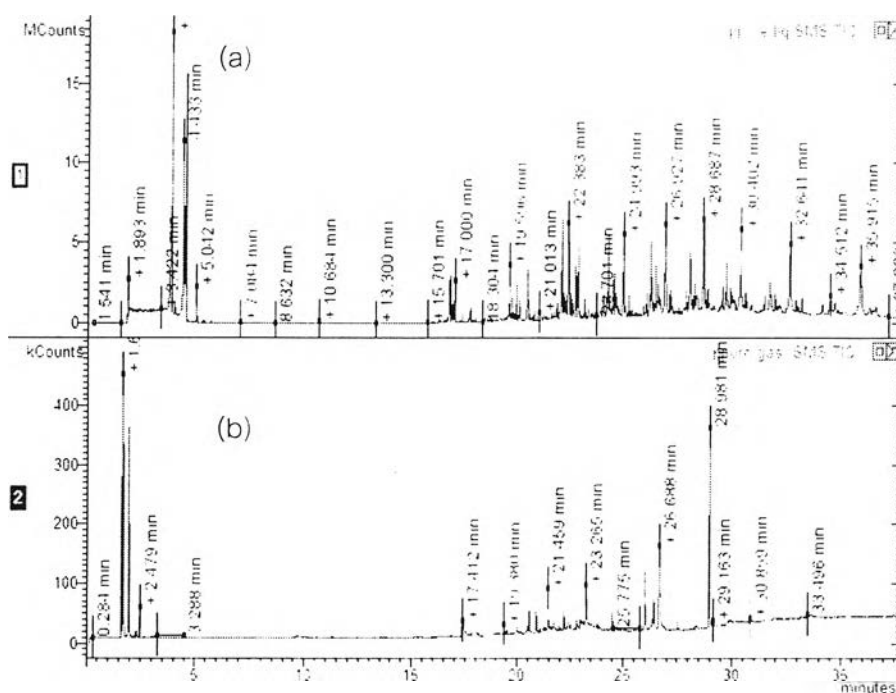


Figure 4.7 Gas chromatograms of PP liquid yield (a) compared with gas yield (b).

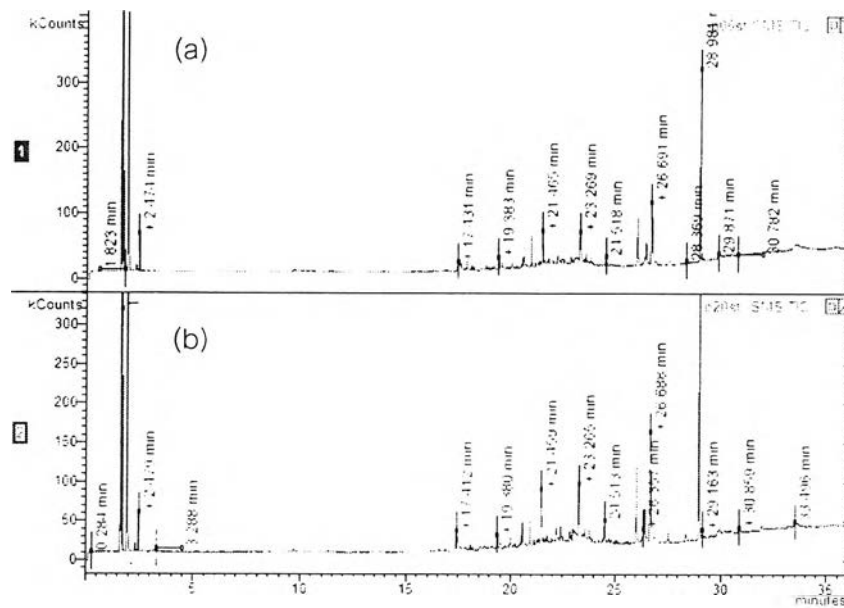


Figure 4.8 Comparison of gas yield from PP composites at 5 (a) and 20% (b) starch contents.

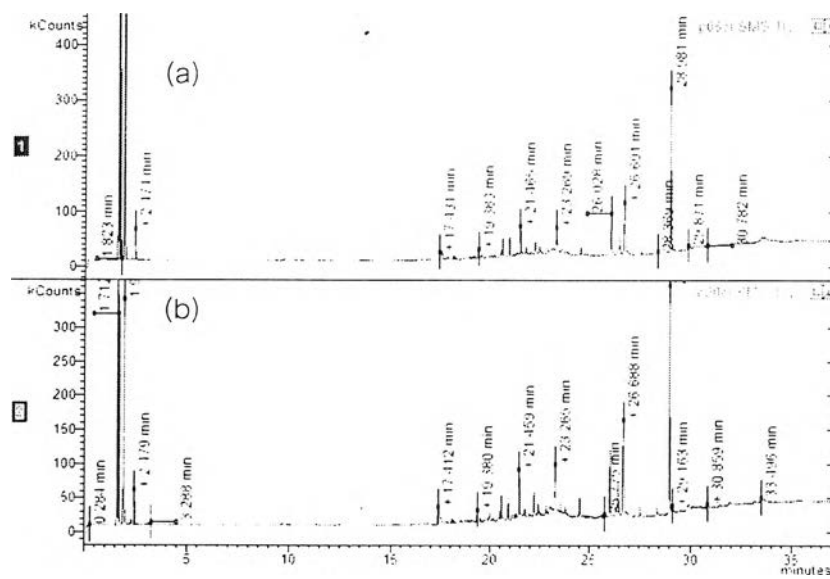


Figure 4.9 Comparison of gas yield from PP composites at 5 (a) and 20% (b) cellulose contents.



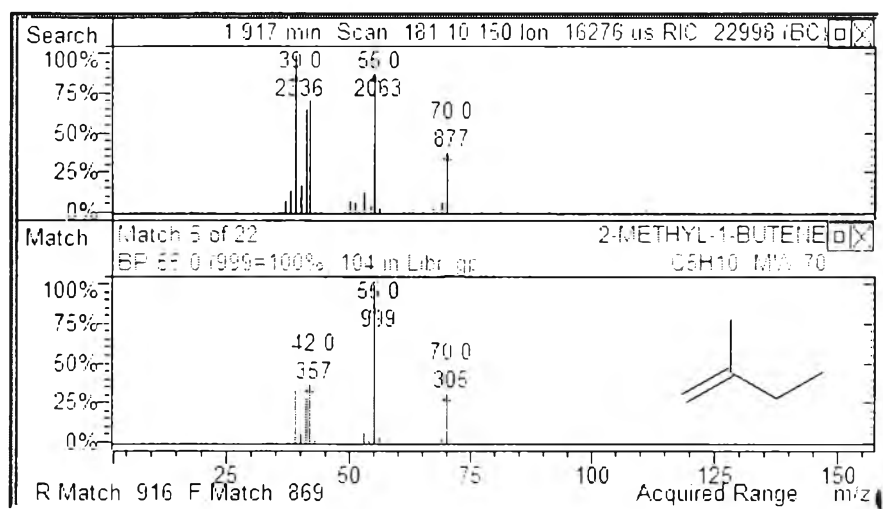


Figure 4.10 Products identification by matched with mass spectrum from library.

Table 4.4 Major constituents of pyrolysis products of PP and PP composites  
(5% additives)

C-Number	Products	Yield% by weight of sample input		
		PP	PP/STR	PP/MCC
3	Propane	0.814	0.804	0.814
	Propene	1.877	1.953	1.943
4	Butane	1.440	1.558	1.506
	Isobutane	0.065	0.105	0.183
	1-butene	1.302	1.365	1.340
5	Pentane	0.796	0.845	0.878
	Isopentane	0.276	0.341	0.309
	2-methyl-1-butene	1.722	1.785	1.770
	1-pentene	0.348	0.348	0.363
6	2-methyl pentane	0.621	0.679	0.660
	2-methyl-1-pentene	2.256	2.370	2.313
	Hexane	0.058	0.116	0.097
	1-hexene	2.237	2.351	2.370
	benzene	0.000	0.070	0.088
7	2,4-dimethyl-1-pentene	3.451	3.274	3.362
	Heptane	2.370	2.280	2.235
	1-heptene	7.034	6.857	6.879
8	4-methyl heptane	3.474	3.371	3.397
	octane	0.618	0.566	0.592
9	2-methyl-1-octene	0.825	0.683	0.654
	2-methyl-4-octane	7.821	7.508	7.537
	2,4-dimethyl-1-heptene	2.901	2.816	2.787
	Cumene	0.000	0.081	0.108
10	2,4,6-trimethyl-1-heptene	6.857	6.668	6.699
	2,4,6-trimethyl-1,6-heptadiene	3.239	3.271	3.208
11	2,6-dimethyl-nonane	5.563	5.352	5.387
12	2,4,6-trimethyl-1-nonene	9.935	9.745	9.670

Table 4.5 Major constituents of pyrolysis products of PP and PP composites  
(10% additive)

C-Number	Products	Yield% by weight of sample input		
		PP	PP/STR	PP/MCC
3	Propane	0.814	0.824	0.834
	Propene	1.877	1.972	1.962
4	Butane	1.440	1.584	1.545
	Isobutane	0.065	0.131	0.196
	1-butene	1.302	1.390	1.378
5	Pentane	0.796	0.861	0.878
	Isopentane	0.276	0.374	0.341
	2-methyl-1-butene	1.722	1.817	1.833
	1-pentene	0.348	0.411	0.395
6	2-methyl pentane	0.621	0.738	0.718
	2-methyl-1-pentene	2.256	2.427	2.332
	Hexane	0.058	0.136	0.155
	1-hexene	2.237	2.389	2.389
	benzene	0.000	0.088	0.106
7	2,4-dimethyl-1-pentene	3.451	3.252	3.384
	Heptane	2.370	2.167	2.212
	1-heptene	7.034	6.835	6.835
8	4-methyl heptane	3.474	3.345	3.422
	octane	0.618	0.540	0.489
9	2-methyl-1-octene	0.825	0.654	0.597
	2-methyl-4-octane	7.821	7.394	7.508
	2,4-dimethyl-1-heptene	2.901	2.759	2.673
	Cumene	0.000	0.108	0.081
10	2,4,6-trimethyl-1-heptene	6.857	6.573	6.604
	2,4,6-trimethyl-1,6-heptadiene	3.239	3.146	3.084
11	2,6-dimethyl-nonane	5.563	5.317	5.352
12	2,4,6-trimethyl-1-nonene	9.935	9.518	9.404

Table 4.6 Major constituents of pyrolysis products of PP and PP composites  
(15% additive)

C-Number	Products	Yield% by weight of sample input		
		PP	PP/STR	PP/MCC
3	Propane	0.814	0.854	0.864
	Propene	1.877	1.991	2.000
4	Butane	1.440	1.610	1.610
	Isobutane	0.065	0.170	0.209
	1-butene	1.302	1.416	1.403
5	Pentane	0.796	0.959	0.926
	Isopentane	0.276	0.390	0.390
	2-methyl-1-butene	1.722	1.864	1.864
	1-pentene	0.348	0.442	0.411
6	2-methyl pentane	0.621	0.757	0.796
	2-methyl-1-pentene	2.256	2.484	2.370
	Hexane	0.058	0.194	0.214
	1-hexene	2.237	2.408	2.427
	benzene	0.000	0.141	0.123
7	2,4-dimethyl-1-pentene	3.451	3.185	3.274
	Heptane	2.370	2.122	2.144
	1-heptene	7.034	6.747	6.702
8	4-methyl heptane	3.474	3.268	3.319
	octane	0.618	0.463	0.412
9	2-methyl-1-octene	0.825	0.569	0.569
	2-methyl-4-octane	7.821	7.366	7.451
	2,4-dimethyl-1-heptene	2.901	2.673	2.616
	Cumene	0.000	0.163	0.217
10	2,4,6-trimethyl-1-heptene	6.857	6.415	6.510
	2,4,6-trimethyl-1,6-heptadiene	3.239	3.053	2.928
11	2,6-dimethyl-nonane	5.563	5.176	5.247
12	2,4,6-trimethyl-1-nonene	9.935	9.404	9.290

Table 4.7 Major constituents of pyrolysis products of PP and PP composites  
(20% additive)

C-Number	Products	Yield% by weight of sample input		
		PP	PP/STR	PP/MCC
3	Propane	0.814	0.884	0.874
	Propene	1.877	2.019	2.029
4	Butane	1.440	1.636	1.650
	Isobutane	0.065	0.223	0.249
	1-butene	1.302	1.441	1.441
5	Pentane	0.796	0.991	1.008
	Isopentane	0.276	0.423	0.455
	2-methyl-1-butene	1.722	1.896	1.928
	1-pentene	0.348	0.490	0.458
6	2-methyl pentane	0.621	0.835	0.815
	2-methyl-1-pentene	2.256	2.541	2.427
	Hexane	0.058	0.233	0.252
	1-hexene	2.237	2.446	2.446
	benzene	0.000	0.176	0.141
7	2,4-dimethyl-1-pentene	3.451	3.075	3.207
	Heptane	2.370	2.054	2.077
	1-heptene	7.034	6.658	6.592
8	4-methyl heptane	3.474	3.191	3.268
	octane	0.618	0.360	0.360
9	2-methyl-1-octene	0.825	0.483	0.483
	2-methyl-4-octane	7.821	7.309	7.366
	2,4-dimethyl-1-heptene	2.901	2.588	2.474
	Cumene	0.000	0.244	0.271
10	2,4,6-trimethyl-1-heptene	6.857	6.352	6.446
	2,4,6-trimethyl-1,6-heptadiene	3.239	2.928	2.803
11	2,6-dimethyl-nonane	5.563	5.106	5.106
12	2,4,6-trimethyl-1-nonene	9.935	9.253	9.139

The comparison of morphology of char residue remained in the sample holder after pyrolysis experiment of biodegradable composites was observed using scanning electron microscopy as seen in Figure 4.11. The char formed by starch exhibited a cracked surface caused by thermal decomposition of weak  $\alpha$ -(1,6)-linkage at branch-points of amylopectin. In contrast, char from cellulose preferred size reducing behavior from averaged diameter about 10 to 5  $\mu\text{m}$  and from averaged length of 60  $\mu\text{m}$  to 30 $\mu\text{m}$ , while the overall morphology was endurance. It might be due to the bond breaking of functional group of cellulose repeating unit instead of damaged in  $\beta$ -(1,4)-linkage of cellulose.

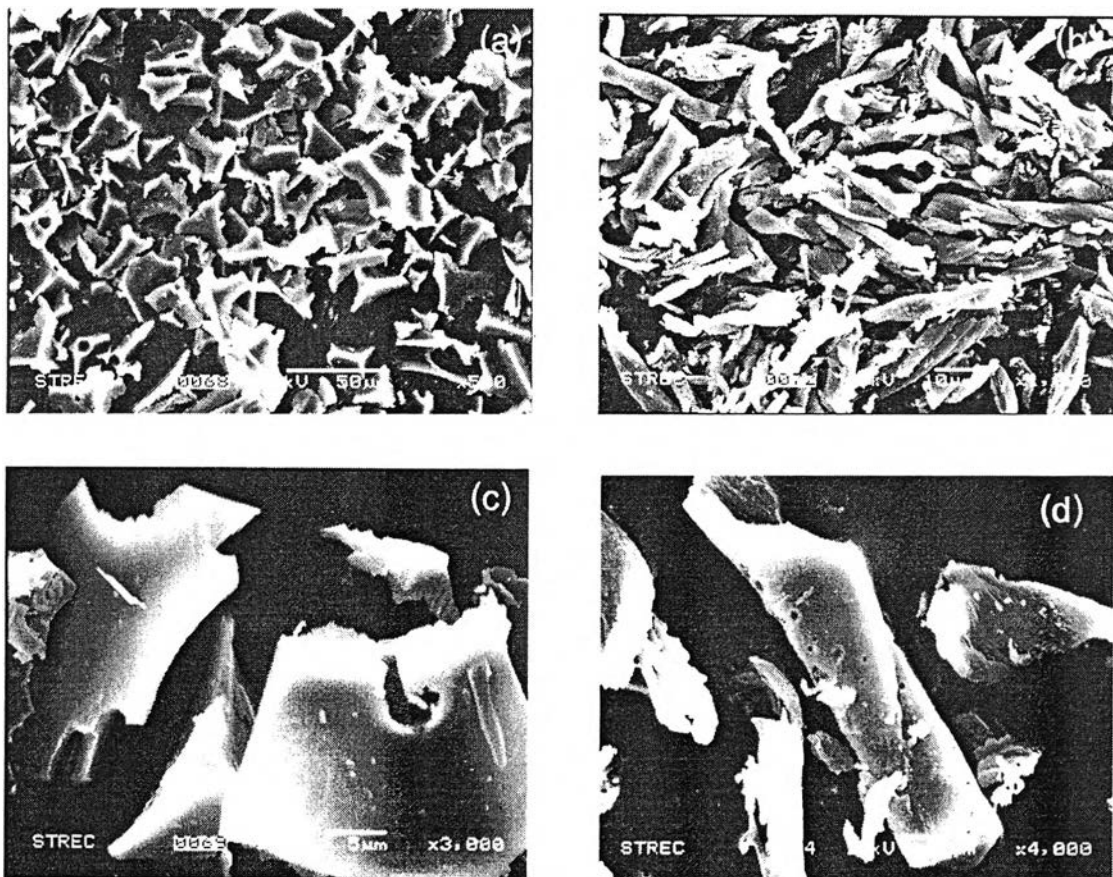


Figure 4.11. Scanning electron micrograph of char residue from PP/STR (a) and PP/MCC (b) composites with a detailed morphology in (c) and (d), respectively

The elemental compositions of char residue were also investigate using elemental analysis technique and summarized in Table 4.8, in order to compare with the compositions occurred from pure starch and cellulose. The results show a large amount of C in char from starch and cellulose was observed, indicating that the other element was cracked and decompose to other volatile products leaving remained C.

Table 4.8 Comparison of elemental composition of starch and cellulose before and after pyrolysis experiment

Elemental composition	Starch (%)		Cellulose (%)	
	before	after	before	after
C	28.05	89.93	29.01	53.97
H	51.42	3.07	49.92	28.53
N	0.14	0.06	0.27	0.05
O	20.08	2.72	20.35	10.48

### 4.2.3 Thermal degradation kinetic studies

Study on rate of reaction of this composite material thermal degradation process is an important part of the appropriate design of actual pyrolysis process if it to be used for dealing with these biodegradable materials. Specifications for sizing, material of construction, reactor profile, and operating conditions for real process must be determined based on these kinetic data.

#### 4.2.3.1 Determination of activation energy

An ordinary differential equation describing the weight loss fraction is given as

$$\frac{d\alpha}{dt} = k_0 \exp(-E_a / RT) \cdot (1 - \alpha)^n \quad (4.1)$$

where,

- $\alpha$  = conversion of the reaction
- $k_0$  = pre-exponential factor
- $E_a$  = the activation energy (kJ/mol)
- $R$  = universal gas constant (8.3136 kJ/mol K)
- $T$  = temperature in Kelvin
- $n$  = reaction order

The fundamental method developed by Friedman is the taking of natural logarithm on both sides of equation 4.1, the equation was in the new form of:

$$\ln\left(\frac{d\alpha}{dt}\right) = \ln k_0 - \frac{E_a}{RT} + n \ln(1 - \alpha) \quad (4.2)$$

By plotting  $\ln\left(\frac{d\alpha}{dt}\right)$  versus  $\frac{1}{T}$ , the curves obtained were linear and the slope of these curves gives us activation energy in the unit of Joules by multiplying with gas constant.

Another technique developed by Ozawa based on an introducing of heating rate ( $\beta = \frac{dT}{dt}$ ) in the experiment. By taking natural logarithm, Eq. 4.1 can be written as



$$\ln \beta = \ln \left( \frac{k_0 (1-\alpha)^n}{d\alpha/dT} \right) - \frac{E_a}{RT} \quad (4.3)$$

The slope from the plot of  $\ln \beta$  against  $\frac{1}{T}$  exhibited a regressed line and the activation energy was observed.

Both Friedman's (Eq. 4.2) and Ozawa's (Eq. 4.3) techniques were used to determine the activation energy of PP. The activation energy of PP at varying heating rate from 10 to 30°C/min obtained by the Friedman's technique by plotting  $\ln(d\alpha/dt)$  against  $1/T$  shown in Figure 4.12 is 296 kJ/mol. Table 4.9 summarized the calculation of slope to achieve the activation energy using Friedman's method.

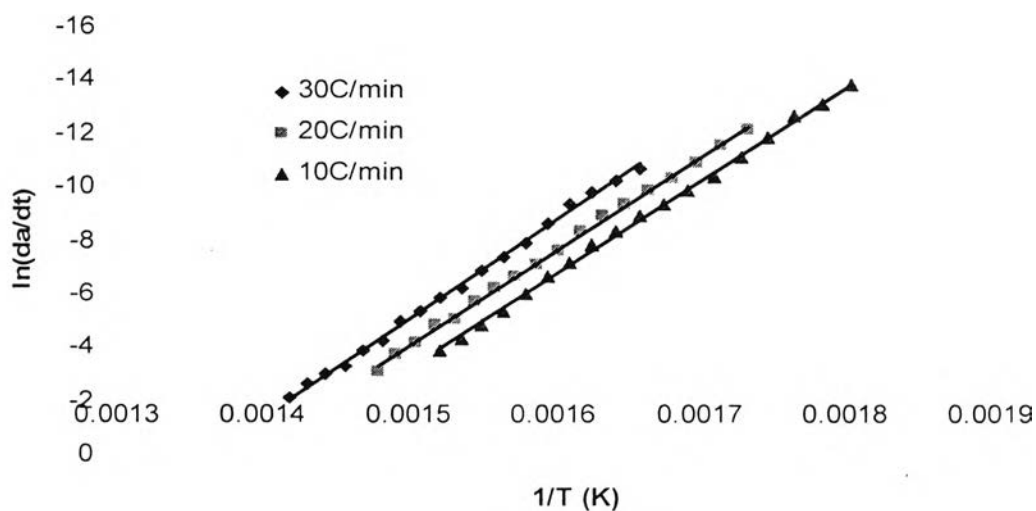


Figure 4.12. Friedman's plot of pure PP at varying heating rates to determine the activation energy.

Table 4.9 Activation energy calculation from slope of Friedman's technique

Heating rate (°C/min)	Linear equation	Slope from equation	$E_a$ after multiply by gas constant (J)
10	$y = -35145x + 49.569$	35145	305119.4
20	$y = -34943x + 48.379$	34943	290725.8
30	$y = -36673x + 49.992$	36673	292406.4
			Average 296.08 kJ/mol

While the Ozawa's technique based on plotting of  $\ln(\beta)$  versus  $1/T$  at degree of conversions varying from 20-80% shown in Figure 4.13 yielding activation energy value of 263.67 kJ/mol. The detail of activation energy obtained was similar to the calculation carried out in Friedman's technique and displayed in Table 4.10.

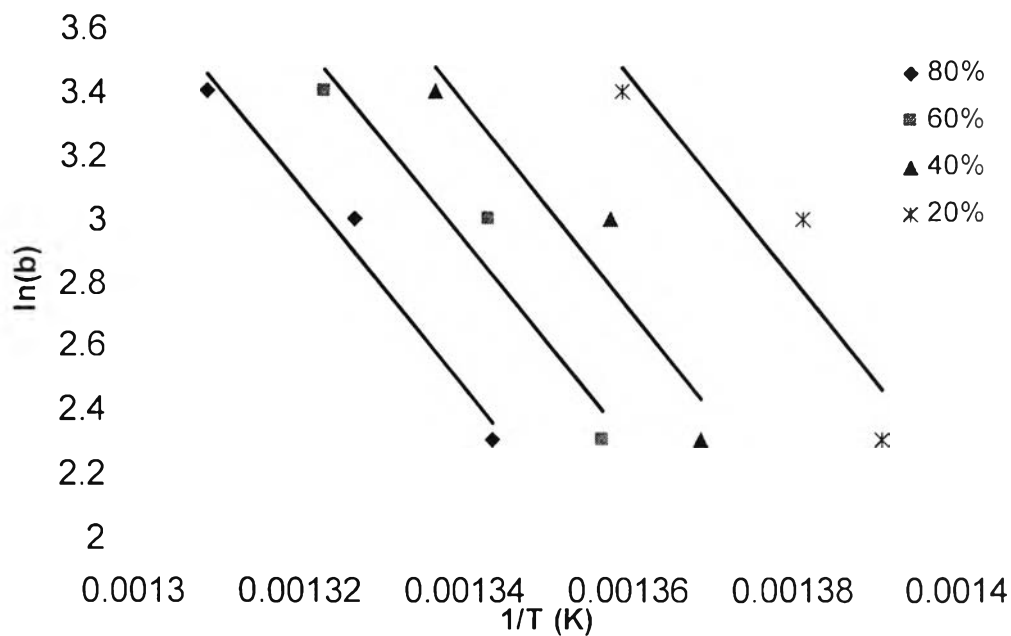


Figure 4.13. Ozawa's plot of pure PP at varying %conversion to determine the activation energy.

Table 4.10 Activation energy calculation from slope of Ozawa's technique

% conversion	Linear equation	Slope from equation	$E_a$ after multiply by gas constant (J)
20	$y = -31717x + 46.576$	31717	263885.4
40	$y = -31714x + 45.851$	31714	263860.5
60	$y = -31488x + 45.125$	31488	262071.7
80	$y = -31832x + 45.118$	31832	264842.2
			Average 263.67 kJ/mol

In summary, the activation energy obtained from both Friedman and Ozawa's technique are 296.08 and 263.67 kJ/mol, respectively. This data is comparable to the activation energy of PP reported by Wielage *et al.*, (1999) with the value of 271.46 kJ/mol. The difference in the values of activation energy can be attributed to the properties of polymer, processing technique, and data determination method. Activation energy obtained by Ozawa's plot seems to be more deviation, because of the regressed line equation was obtained from only three data points of heating rate plot.

Similarly, the activation energy of PP obtained from the PP/STR and PP/MCC composites were determined based on the Friedman's technique at a constant heating rate of 10°C/min. Figure 4.14 and 4.15 show the Friedman plot which used to calculate the activation energy of PP/STR and PP/MCC composites from the slope of the regressed line of  $\ln\left(\frac{d\alpha}{dt}\right)$  versus  $\frac{1}{T}$ . The values obtained are also shown in Table 4.11. The activation energy of PP in biodegradable composites shows lower values than that of pure components. It can be inferred that the presences of biodegradable additives lessen thermal stability and promote the thermal decomposition of PP. The influence of starch on the activation energy of PP was more pronounced by lowering  $E_a$  of PP from 296.1 to 242.7 in 20% starch content compared with the value of 260.74 in 20% cellulose content. It might be due to more char produced from starch which promotes the bond breaking of PP. The similar trends can be observed with the increasing of additive contents which can be described by the same assumption.

Table 4.11 The activation energy of PP in PP/STR and PP/MCC composites

Sample	Activation energy (kJ/mol)	
	PP/STR	PP/MCC
0%	296.08	
5%	265.53	280.83
10%	256.65	266.73
15%	255.57	261.35
20%	242.71	260.74

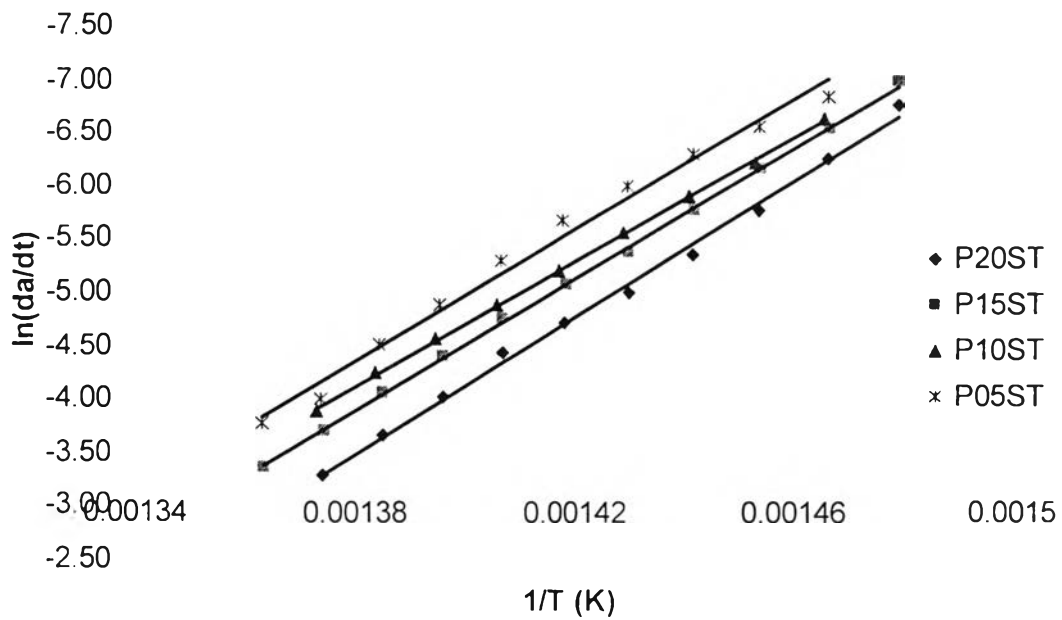


Figure 4.14. Friedman's plot of PP component in PP/STR composites to determine the activation energy at a heating rate of  $10^{\circ}\text{C}/\text{min}$ .

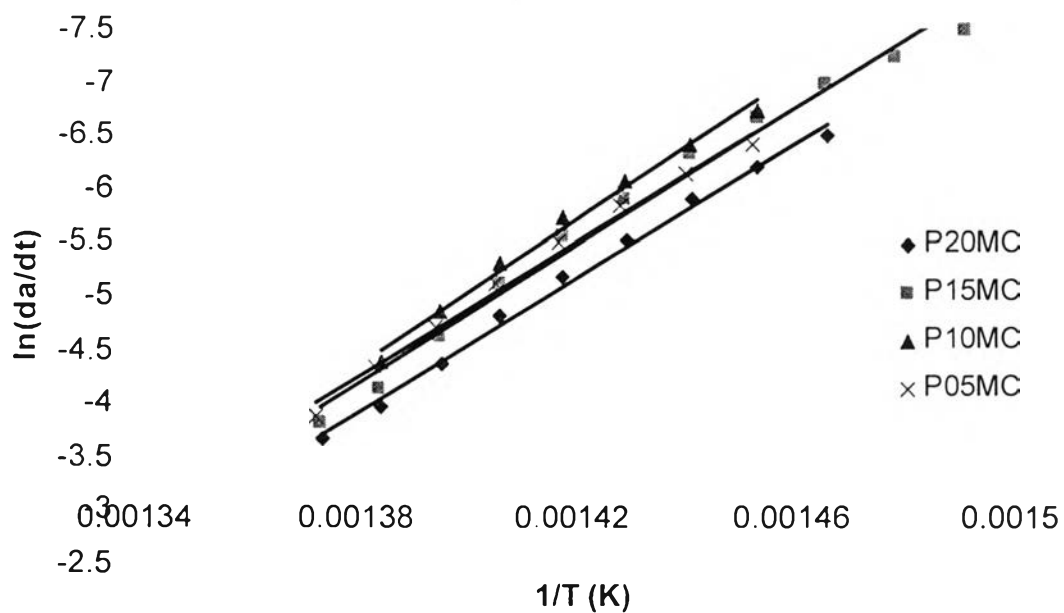


Figure 4.15. Friedman's plot of PP component in PP/MCC composites to determine the activation energy at a heating rate of  $10^{\circ}\text{C}/\text{min}$ .

The activation energy of starch and cellulose in PP composites was also observed using Friedman's technique as shown in Figure 4.16 and 4.17. The conclusion of activation energy of biodegradable additives in varied contents was shown in Table 4.12. The activation energy of starch is greater than cellulose, so starch is more thermally stable.

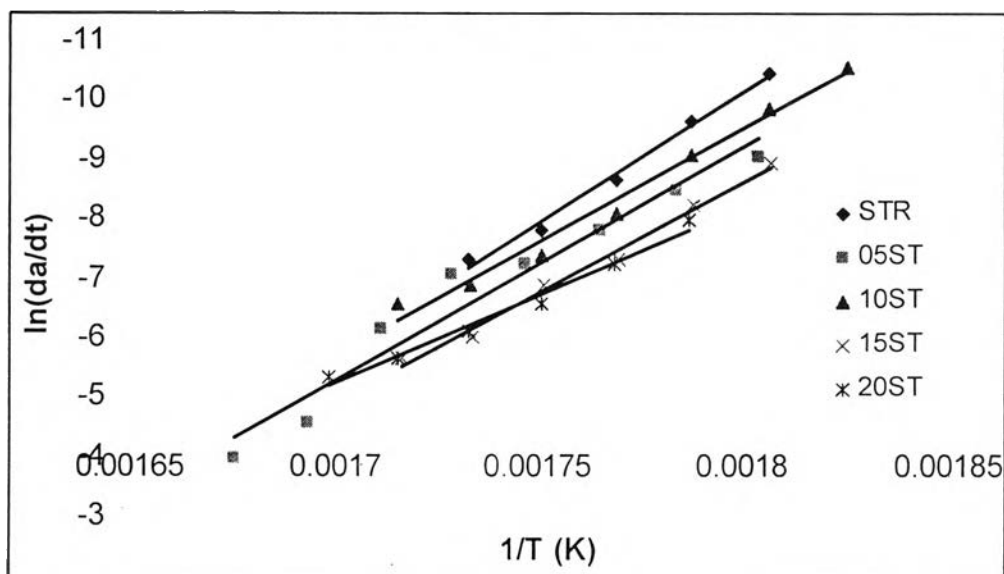


Figure 4.16. Friedman's plot of starch component in PP/STR composites to determine the activation energy at a heating rate of  $10^{\circ}\text{C}/\text{min}$ .

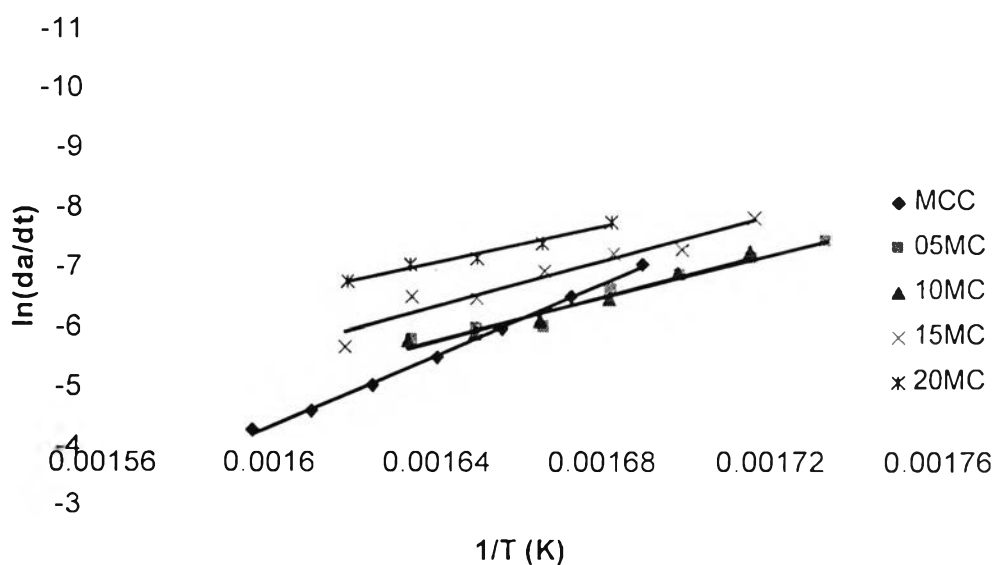


Figure 4.17. Friedman's plot of cellulose component in PP/MCC composites to determine the activation energy at a heating rate of  $10^{\circ}\text{C}/\text{min}$ .

Table 4.12 The activation energy of starch and cellulose at various content

Sample	Activation energy (kJ/mol)	
	STR	MCC
0%	370.02	233.43
5%	322.72	145.69
10%	318.06	137.63
15%	308.76	135.72
20%	246.20	135.49

#### 4.2.3.2 Determination of other kinetic parameters

The rearrangement of equation 4.1 resulting in the form of

$$\frac{d\alpha / dt}{\exp(-E_a / RT)} = k_0 \cdot (1 - \alpha)^n \quad (4.4)$$

By taking natural logarithm on both side of Eq. 4.4, it can be written as

$$\ln \left[ \frac{(d\alpha / dt)}{\exp(-E_a / RT)} \right] = \ln k_0 + n \ln(1 - \alpha) \quad (4.5)$$

By plotting of  $\ln \left[ \frac{(d\alpha / dt)}{\exp(-E_a / RT)} \right]$  against  $\ln(1 - \alpha)$  in an equation 4.5 with the activation energy from Friedman's plot in section 4.2.3.1, the other kinetic parameter ( $n, k_0$ ) was obtained from slope equal to  $n$  (reaction order or how many species occurred during reaction) and an intercept equal to  $\ln k_0$  (pre-exponential factor or rate constant at infinite temperature) as shown in Figure 4.18 and 4.19. The results are summarized in Table 4.13. It can be seen that the value of  $n$  and  $k_0$  were corresponded to the increase of additive contents. When compare the effect of starch with cellulose, it can be seen that starch provoked more influence on these kinetic data.

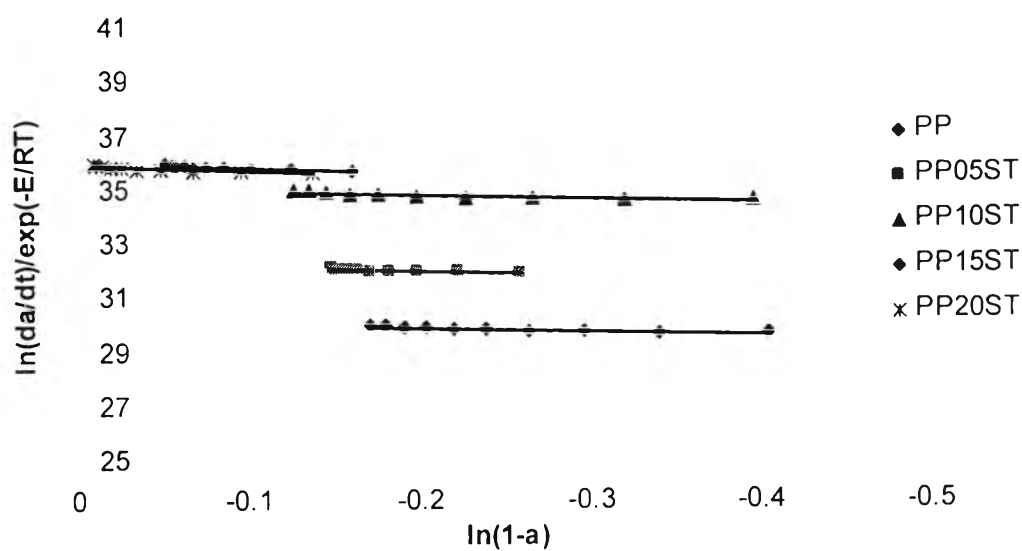


Figure 4.18 Reaction order ( $n$ ) and pre-exponential factor ( $k_0$ ) determination of PP component in PP/STR composites..

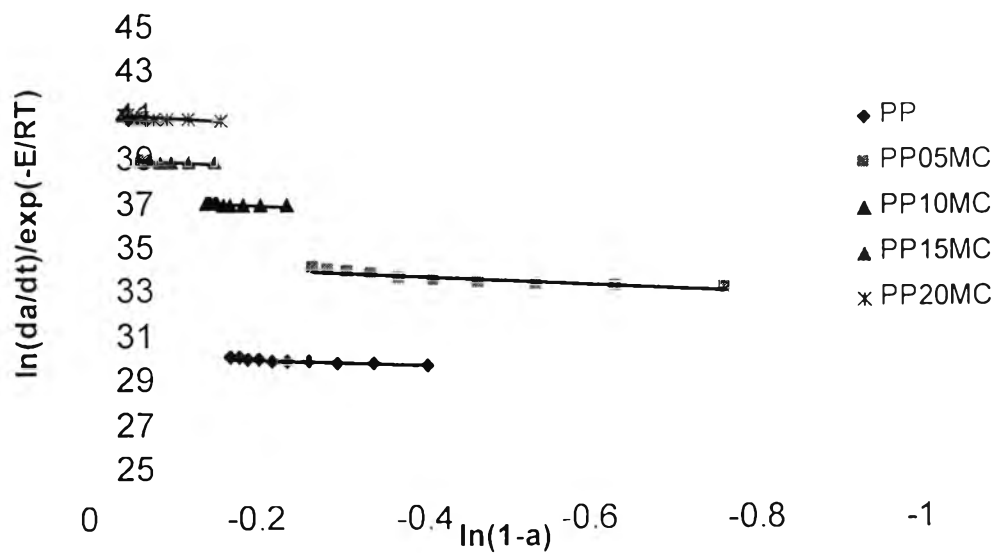


Figure 4.19 Reaction order ( $n$ ) and pre-exponential factor ( $k_0$ ) determination of PP component in PP/MCC composites..

Table 4.13 Kinetic parameter for the thermal decomposition of PP

Sample	PP/STR		PP/MCC	
	$n$	$\ln k_0$	$n$	$\ln k_0$
0%	$n = 1.51$		$\ln k_0 = 30.20$	
5%	1.54	32.29	1.51	34.35
10%	1.60	35.12	1.88	37.21
15%	2.36	36.07	2.10	39.08
20%	2.62	35.94	2.21	41.04